



Thermogravimetric analysis–mass spectrometry (TGA–MS) of hydromagnesite from Dujiali Lake in Tibet, China

Yongjie Lin^{1,2} · Mianping Zheng^{1,2} · Chuanyong Ye¹  · Ian M. Power³

Received: 11 December 2017 / Accepted: 11 March 2018 / Published online: 31 March 2018
© Akadémiai Kiadó, Budapest, Hungary 2018

Abstract

Thermogravimetric analysis–mass spectrometry, in situ X-ray diffraction, scanning electron microscopy and Fourier transform infrared spectroscopy were used to characterize hydromagnesite $[\text{Mg}_5(\text{CO}_3)_4(\text{OH})_2 \cdot 4\text{H}_2\text{O}]$ from Dujiali Lake in Tibet, China. This study describes the variations in the thermal decomposition mechanisms of hydromagnesite at varying heating rates and under either helium (He) or carbon dioxide (CO_2) atmospheres. In a He atmosphere, only two decomposition stages were observed; the loss of the crystalline water followed by the combined dehydroxylation and decarbonation. However, under a CO_2 atmosphere, the dehydroxylation and decarbonation occur separately as the inert CO_2 gas prevents the decomposition of the MgCO_3 component of hydromagnesite. Overall, the thermal decomposition is an endothermic process. A distinctly exothermic process occurs at about 540 °C under conditions of high partial pressure of CO_2 or high heating rate and implies the crystallization of magnesite (MgCO_3). We propose that the release of H_2O and CO_2 at different stages likely results from the complicated hydrogen bonds and different carbonate groups in the crystal structure of hydromagnesite.

Keywords Hydromagnesite · TGA–MS · Thermal decomposition · In situ XRD · FT-IR

Introduction

Hydromagnesite $[\text{Mg}_5(\text{CO}_3)_4(\text{OH})_2 \cdot 4\text{H}_2\text{O}]$ forms at Earth's surface conditions and is one of the most common magnesium carbonate minerals found in nature, especially in carbonate playas [1–4]. During the past decades, extensive

research has been conducted on the thermal decomposition of hydromagnesite to study its structural features, main physical and chemical properties [5–18], and to better understand its industrial application as a fire retardant [19–23]. For example, Padeste et al. [11] conducted an analysis of the thermal decomposition of hydromagnesite under nitrogen (N_2), hydrogen (H_2), and carbon dioxide (CO_2) atmospheres. Additionally, Khan et al. [16] found that procedural variables including atmospheric conditions and heating rating affect the origin of the exothermic peak of hydromagnesite during the decomposition process. Recently, Hollingbery and Hull [23] summarized the current state of knowledge regarding the thermal decomposition of hydromagnesite. Despite numerous investigations into the thermal decomposition of hydromagnesite, there remain uncertainties. For example, the cause of an exothermic event at just above 500 °C under some specific conditions remains uncertain with at least two explanations being proposed [7, 8, 18, 23]. Khan et al. [16] suggest that this exothermic event is due to mechanical stress within the crystal structure caused by the release of CO_2 which becomes trapped, while Sawada et al. [7, 8, 18, 24] attribute

✉ Mianping Zheng
zhengmp2010@126.com

✉ Chuanyong Ye
yechuanyong@cags.ac.cn

Yongjie Lin
linyongjie2014@163.com

Ian M. Power
ianpower@trentu.ca

¹ Institute of Mineral Resources, Chinese Academy of Geological Sciences, No. 26, Baiwanzhuang Street, Beijing 100037, China

² School of Earth Sciences and Resources, China University of Geosciences, No. 29, Xueyuan Road, Beijing 100083, China

³ Trent School of the Environment, Trent University, 1600 West Bank Drive, Peterborough, ON K9L 0G2, Canada

this exotherm to the crystallization of magnesium carbonate.

Thermal analysis using thermogravimetric techniques has proven very useful for determining the stability of minerals, such as the mass loss steps, the temperature of the mass loss, and the mechanism for the mass loss [25–30]. These thermoanalytical techniques have been used to study several complex minerals including hydromagnesite [11, 14, 26]. More recently, a novel method of equivalent characteristic spectrum analysis (ECSA) was developed to analyze the mass spectrum of thermogravimetry analysis–mass spectrometry system according to the operating principle of TGA–MS coupling system [31]. This method can effectively separate the mass and eliminate the mass discrimination and temperature-dependent effect, even though there may be overlapping of characteristic peaks. Using this analytical technique to study the decomposition mechanisms of hydromagnesite, we performed a series of TGA/MS experiments on hydromagnesite samples under He and CO₂ atmospheres at heating rates of 5, 10, 15, and 20 °C min⁻¹, respectively. The decomposition mechanism of hydromagnesite has been disclosed due to mass spectrometry analysis of the volatiles formed during decomposition. This study describes the variations in the thermal decomposition mechanisms of hydromagnesite at varying heating rates and under either He or CO₂ atmospheres.

Experimental

Materials

Hydromagnesite deposits were found in the first lake terrace of the northwest of Dujiali Lake during a field survey in March 2015 [3]. The hydromagnesite sediments directly overlay Quaternary sediments in the lake terrace, which was subparallel to the land surface and around 10 m thick above the present lake surface. After removal of the weathered surface crust, a representative sample was taken from the DPSP01 profile through the hydromagnesite deposit. The hydromagnesite samples were analyzed directly after crushing without prior size fraction separation since one of the objectives was to remove the effect of the particle size on the experiments.

Scanning electron microscopy

SEM was carried out at the Centre for High-Throughput Phenogenomics at The University of British Columbia, Canada. Samples were mounted onto aluminum stubs using 12-mm carbon adhesive tabs and coated iridium (10 nm) using a Leica EM MED020 coating system. Imaging was performed using an FEI Helios NanoLab 650 emission

SEM operating voltage of 1.0 kV to produce high-resolution images.

Fourier transform infrared spectroscopy

FT-IR spectroscopy of the hydromagnesite sample was performed by direct transmittance using the KBr pellet technique. Spectra were recorded in the range of 4500–400 cm⁻¹ using a Spectrum 100 FT-IR spectrometer (PerkinElmer Inc., USA). Aliquots (around 1 mg) of each powdered hydromagnesite sample were diluted with 100 mg of vacuum-dried KBr powder and subjected to a pressure of 10 tonnes, and then tableting the mixture of hydromagnesite and KBr into a very thin film with a diameter of 13 mm was performed. All the spectra were measured at a spectral resolution of 4 cm⁻¹, and 16 scans were signal-averaged in each interferogram.

In situ X-ray diffraction

XRD patterns were collected on a Rigaku SmartLab X-ray diffractometer with Cu K α radiation. The high-temperature experiments were performed using an X-ray reactor chamber HTK1200 Anton Paar, in which the scan rate was 5° min⁻¹, and the XRD patterns were recorded in a reducing atmosphere. The intensity data were collected in a 2 θ range from 5 to 80° with a scan rate of 5° min⁻¹ in the temperature range of 50–800 °C. The data were collected at the intervals of 50 °C, and each test point was stopped for 3 min under constant temperature. In this chamber, the gas flow (H₂, N₂) was forced through the sample packed on a sintered glass sieve and placed in the center of an oven, and the heating rate at 5 °C min⁻¹.

Thermogravimetric analysis/mass spectrometry

The TGA/MS experiments were performed at the Institute of Engineering, Thermophysics, Chinese Academy of Sciences, using a Rigaku Thermo Mass Photo thermogravimetric analysis instrument in a flow of pure He and mixed flowing gases atmosphere (He and CO₂) at atmospheric pressure. Under He atmospheric conditions, approximately 10 mg of each sample underwent thermal analysis and were heated from 25 to 900 °C with a flow rate of 300 mL min⁻¹ at a heating rate of 5, 10, 15, and 20 °C min⁻¹, respectively. In addition, 10 mg of each powdered hydromagnesite sample was diluted with 3 mg of calcium sulfite (CaSO₃) and subjected to thermal analysis (25–900 °C) at a heating rate of 20 °C min⁻¹ in pure flowing He atmosphere. In CO₂ atmosphere condition, the concentration of CO₂ was controlled to 5% with a helium flow rate of 285 mL min⁻¹ and a CO₂ flow rate of 15 mL min⁻¹. Approximately 10 mg of each sample

underwent thermal analysis and were heated from 25 to 900 °C at a heating rate of 10 and 20 °C min⁻¹, respectively. The qualitative analysis of the mass spectrum at an arbitrary temperature can be automatically performed by directly linking to the NIST-MS Library Search software, and we can understand complex multistage reactions and translational reactions through simultaneous measurements of dynamic TGA and MS. The method of equivalent characteristic spectrum analysis (ECSA) is to analyze the mass spectrum of TGA/MS system according to a study by Xia et al. [31].

Results and discussion

Microscopy and spectroscopy

In hand specimen, the hydromagnesite samples were bright white, dry, and clay-like. The detailed morphologies of the hydromagnesite sediments were investigated using SEM (Fig. 1). The sediments were comprised of interlocking crystals of hydromagnesite, and the hydromagnesite crystals generally had a platy crystal morphology (Fig. 1a) or occasionally a flakey crystal morphology (Fig. 1b).

The crystal structure of hydromagnesite is based on a three-dimensional framework of corrugated layers of MgO₆ octahedra and triangles of carbonate ions [32, 33]. The hydroxyl group is shared by three MgO₆ octahedra, while the water molecule is located at an unshared corner of an MgO₆ octahedra. The FT-IR hydromagnesite spectrum shows bands at approximately 796 (the strongest one), 853, and 885 cm⁻¹ that correspond to the carbonate (CO₃²⁻) bending vibration (Fig. 2). An absorption band at approximately 1119 cm⁻¹ is due to CO₃²⁻ symmetric stretching vibration. Carbonate ion in the hydromagnesite exists as bicarbonate, and a strong band that is splitting into two around 1423 and 1483 cm⁻¹ corresponds to the asymmetric stretching vibrations of bicarbonate ions

[34, 35]. Two crystallographically distinct types of carbonate ions exist in the hydromagnesite structure, which is in accordance with the FT-IR results. The C(I)O₃ ion is considered to be parallel to (001) or (011) of the pseudo-orthorhombic cell, while the C(II)O₃ ion is parallel to the *c*-axis and has an angle of 15° with (100). Furthermore, one oxygen atom in the C(I)O₃ ion coordinates to two Mg atoms and the remaining two oxygen atoms coordinate to one Mg atom, whereas in the C(II)O₃ ion all oxygen atoms coordinate to two Mg atoms [32]. The two absorption bands at approximately 3515 and 3451 cm⁻¹ relate to the water of crystallization. A band at around 1645 cm⁻¹ was attributed the O–H bending mode of water, while a free O–H vibration band is observed at 3649 cm⁻¹. There are three distinct kinds of hydrogen bonds in the hydromagnesite structure: (1) Short O (W11) ...O (11) distance (2.787 Å) indicated a strong hydrogen bond. (2) Longer O (W1) ...O (1) and O (W11) ...O (W1) distances (2.787 and 2.844 Å, respectively) indicate a weak hydrogen bond. (3) The O (W1) water molecule shows a very long (3.110 Å) and bent (141°) O ...O contact with O (W11), indicating a very weak hydrogen bond [33]. Thus, FT-IR analysis confirms the chemical composition and physical state of the hydromagnesite, and thus, the structure and composition of hydromagnesite [34–37].

In situ X-ray diffraction

The XRD patterns of hydromagnesite at different temperatures are shown in Fig. 3. The crystalline phases were identified in comparison with The International Centre for Diffraction Data files. The diffraction peaks of hydromagnesite gradually decreased with increasing calcination temperature and demonstrate that hydromagnesite changes from a crystalline phase to an amorphous state. The diffraction peak heights of hydromagnesite decreased at a temperature of 250 °C and were completely unrecognizable at approximately 350 °C. One of the diffraction peaks

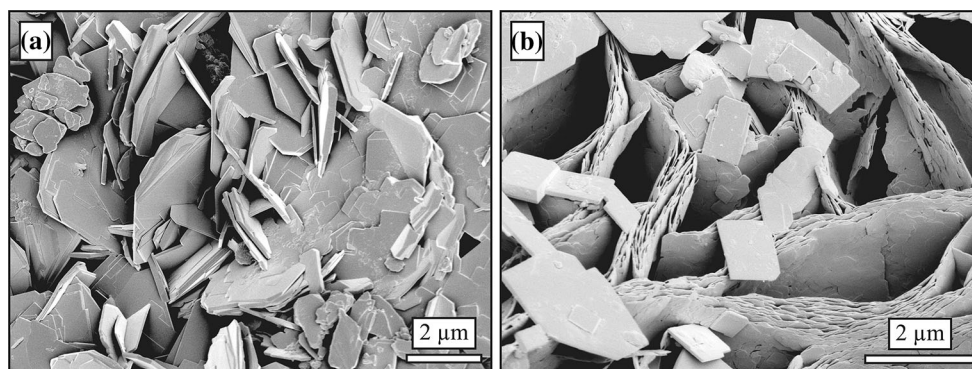


Fig. 1 Representative SEM micrographs of Dujiali Lake hydromagnesite. Micrographs showing hydromagnesite with predominately platy (a) and flakey (b) crystals morphologies

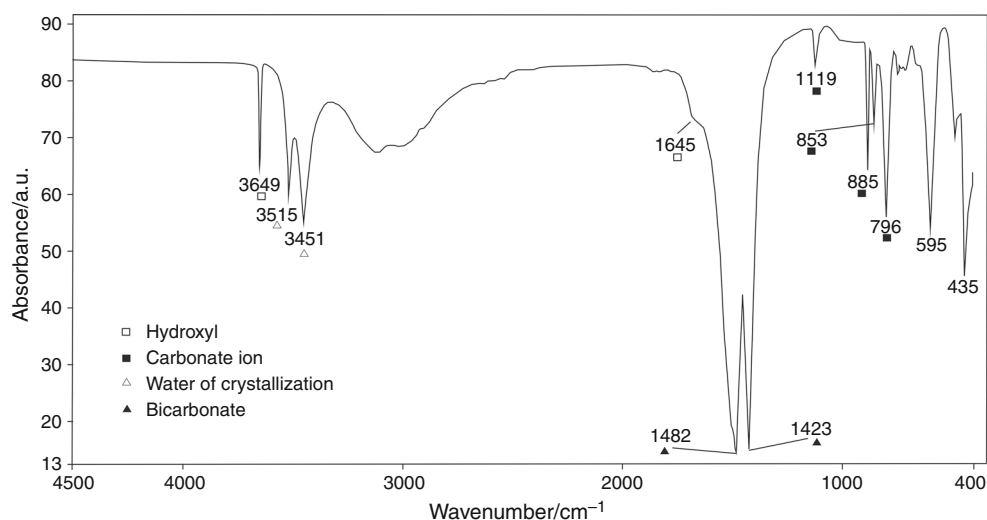


Fig. 2 FT-IR spectrum of hydromagnesite samples

($2\theta = 42^\circ$) of periclase (MgO) appeared at 350°C while most of its other peaks appeared when the temperature

reached 550°C . The XRD pattern confirmed the phase transformation of hydromagnesite samples at a heating rate of 5°C min^{-1} , and hydromagnesite sample contained a small amount of aragonite.

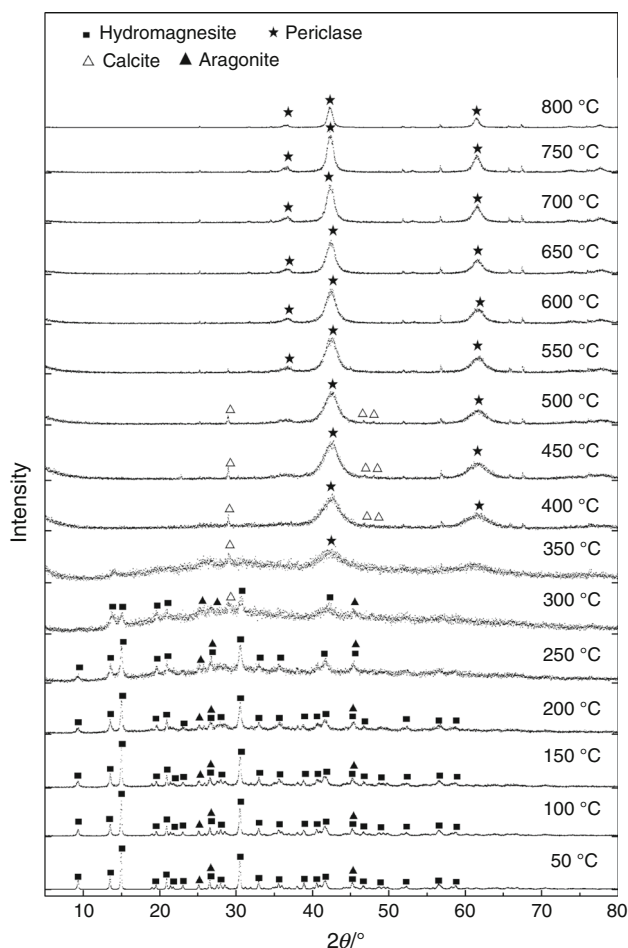


Fig. 3 In situ high-temperature XRD patterns of hydromagnesite samples from 50 to 800°C

Thermal decomposition mechanism of hydromagnesite

The DTG curves and analysis of the outlet gases (CO_2 and H_2O) of hydromagnesite at the heating rates of $10^\circ\text{C min}^{-1}$ in He atmosphere are presented in Fig. 4. The coupled TGA–MS analysis revealed that the evolved gases are water (H_2O) and carbon dioxide (CO_2). The relationship between mass flow rate and temperature of evolved gases with various heating rates is presented in Fig. 5. Three prominent mass losses are observed in the temperature range of 200 – 350 , 350 – 550 , and 550 – 650°C . The first mass loss was approximately 14.65% followed by losses of 32.76% and 6.9% for the second and third mass losses, respectively, when the measurements were carried out at a heating rate of $10^\circ\text{C min}^{-1}$. During those decomposition stages, approximately 59.5% of the original hydromagnesite was released as CO_2 and H_2O . The theoretical mass loss based upon the ideal hydromagnesite formula is 60.52% due to decarbonation (37.77%), water loss (15.45%), and hydroxyl unit loss (7.30%). Two prominent H_2O release steps were observed, while a very weak H_2O release step occurs at around 500°C (Fig. 5), and most of the evolved H_2O gas released in first mass loss stage, while there was almost no CO_2 gas released in this stage (200 – 350°C). There are three distinct kinds of hydrogen bonds in the crystal structure of hydromagnesite, which can be corresponded to the three prominent H_2O release stages. Thus, it is reasonable to conclude that the

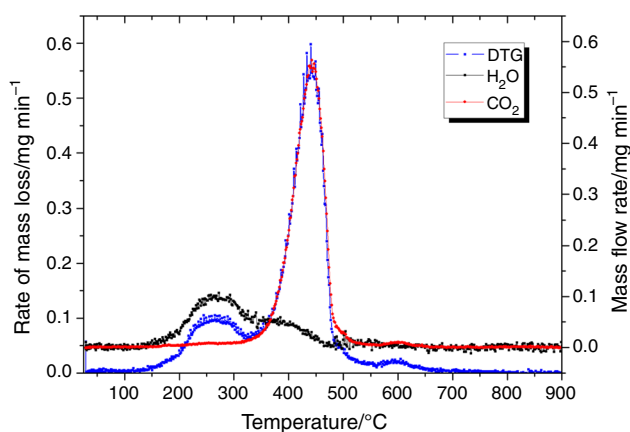
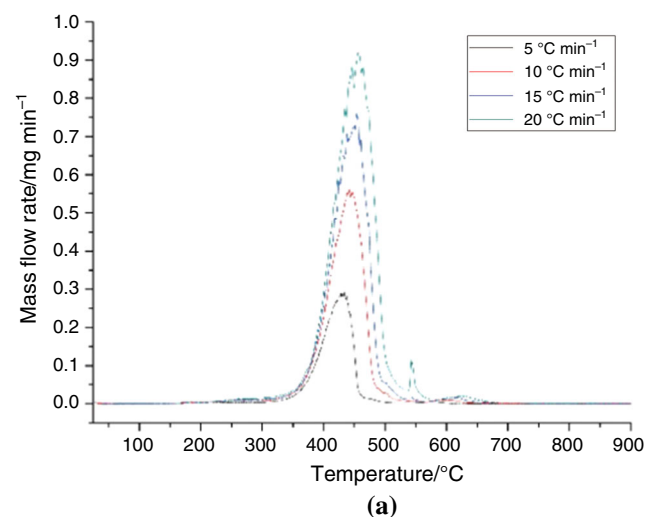


Fig. 4 DTG curves and analysis of the outlet gases (CO_2 and H_2O) from the decomposition of hydromagnesite samples at a heating rate of $10\text{ }^\circ\text{C min}^{-1}$ in a helium atmosphere from 25 to $900\text{ }^\circ\text{C}$

first decomposition stage is related to the dehydration (release of water of crystallization), while the second mass loss stage ($350\text{--}550\text{ }^\circ\text{C}$) is the combination of dehydroxylation [decomposition of $\text{Mg}(\text{OH})_2$ to MgO] and decarbonation [decomposition of MgCO_3 to MgO]. The dehydroxylation step overlaps with both the dehydration and decarbonation steps. However, it is noted from Fig. 5 that the third mass loss ($550\text{--}650\text{ }^\circ\text{C}$) is attributed to the release CO_2 gas.

An experiment that added CaSO_3 was conducted at a heating rate of $20\text{ }^\circ\text{C min}^{-1}$ under a He atmosphere to elucidate the source of the evolved CO_2 gas in the last step (temperature range of $600\text{--}700\text{ }^\circ\text{C}$; Fig. 6). The thermal decomposition temperature range of CaCO_3 and CaSO_3 is very close, yet the activation energy for the thermal decomposition of CaSO_3 is slightly greater than CaCO_3 .



Given that the thermally decomposed solid product is CaO for both compounds, the added CaSO_3 will interfere with the thermal decomposition of CaCO_3 in the experiment, resulting in the piecewise phenomenon of the release of CO_2 produced by the thermal decomposition of CaCO_3 . It can be suggested that the third release of CO_2 ($550\text{--}650\text{ }^\circ\text{C}$) is due to the decomposition of CaCO_3 , as the hydromagnesite samples contain a small amount of aragonite. Therefore, the first two CO_2 gas release stages in a He atmosphere are attributed to the decomposition of carbonate group in the hydromagnesite structure, as two crystallographically distinct kinds of carbonate ions exist. Overall, it is reasonable to conclude that the decomposition of hydromagnesite occurs in two prominent mass losses in the temperature range of $200\text{--}350$ and $350\text{--}550\text{ }^\circ\text{C}$, respectively.

The TG and DTG curves of hydromagnesite at various heating rates in a CO_2 atmosphere are presented in Fig. 7. The coupled TGA–MS analysis reveals that the evolved gases are H_2O and CO_2 , and the relationship between mass flow rate and temperature of evolved gases with various heating rates is presented in Fig. 8. The thermal decomposition of hydromagnesite is more complex in a CO_2 atmosphere than a He atmosphere. The five detail decomposition steps of hydromagnesite samples were detected at a heating rate of $10\text{ }^\circ\text{C min}^{-1}$, while six detail decomposition steps were detected at a heating rate of $20\text{ }^\circ\text{C min}^{-1}$. Three prominent CO_2 release steps are observed, while the main stage of CO_2 release is observed in the temperature range of $500\text{--}600\text{ }^\circ\text{C}$ because the CO_2 inhibits the decomposition of magnesite. Two prominent H_2O release steps are observed in the temperature range of $200\text{--}300$ and $400\text{--}450\text{ }^\circ\text{C}$, which occur separately with the stage of CO_2 release. The last step has been attributed to the

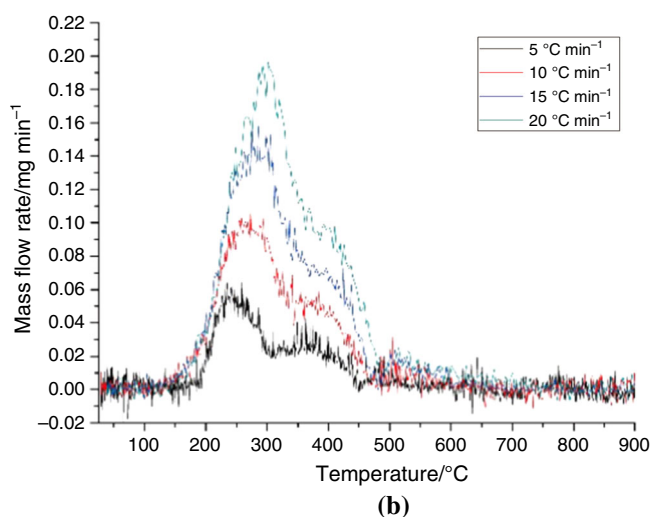


Fig. 5 Analysis of the outlet gases (CO_2 and H_2O) from the decomposition of hydromagnesite in a pure flowing helium atmosphere with different heating rates from 25 to $900\text{ }^\circ\text{C}$. **a** CO_2 . **b** H_2O

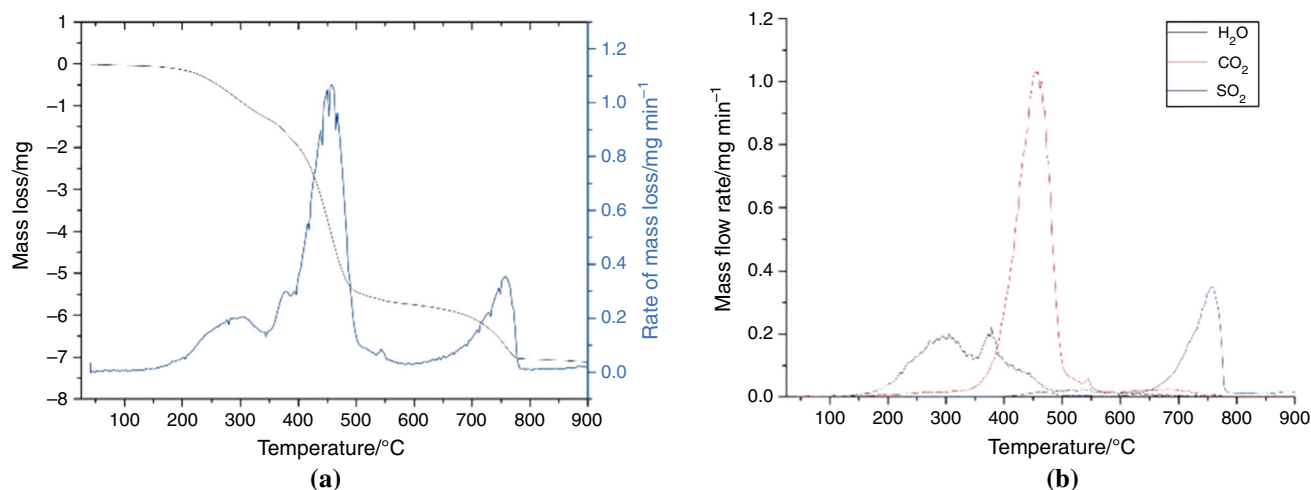


Fig. 6 **a** TG–DTG results of hydromagnesite samples with added calcium sulfite in a helium atmosphere with the heating rate of 20 °C min⁻¹; **b** analysis of the outlet gases (CO₂, H₂O and SO₂) from

the decomposition of hydromagnesite sample with added calcium sulfite from 25 to 900 °C

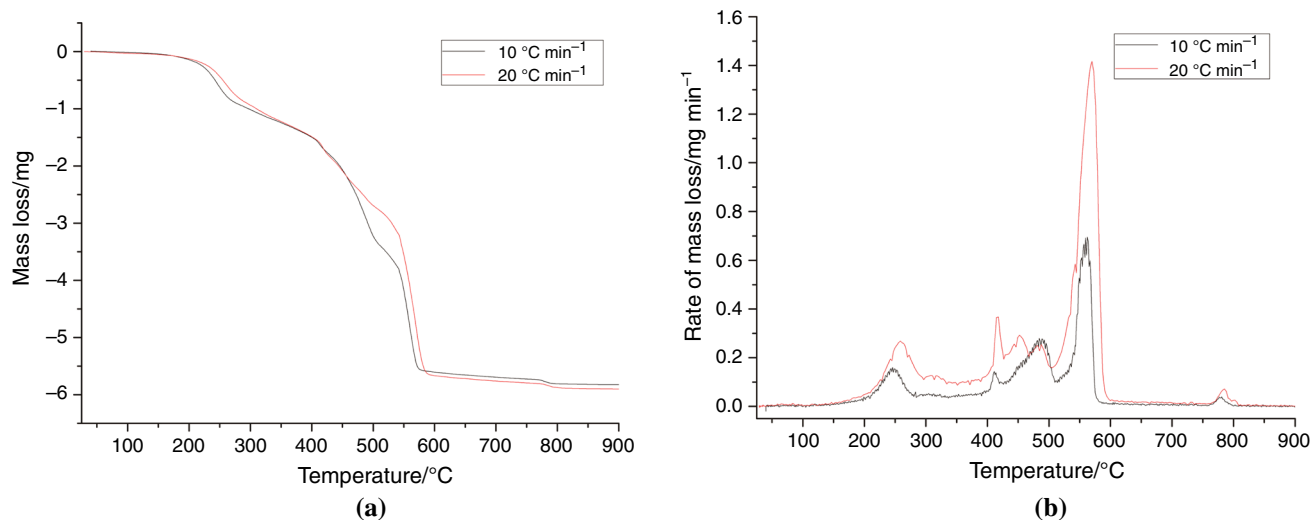


Fig. 7 **a** TG and **b** DTG curves for the decomposition of hydromagnesite samples at various heating rates in a carbon dioxide atmosphere from 25 to 900 °C

decomposition of calcium carbonate. Thus, the dehydroxylation and decarbonation occur separately for hydromagnesite in a CO₂ atmosphere. Overall, the partial pressure of CO₂ significantly affects the decomposition mechanism of hydromagnesite. The decomposition of hydromagnesite occurs in three stages under CO₂ atmosphere as the dehydroxylation and decarbonation occur separately.

Exothermic event in the decomposition of hydromagnesite

This clearly exothermic event has been reported for hydromagnesite at just above 500 °C under some conditions [7, 8, 18, 23], yet its source and the process involved

in its formation are not well understood. Khan et al. [16] suggest that this exothermic event is due to mechanical stress within the crystal structure caused by the release of CO₂ which becomes trapped, while Sawada et al. attribute this exotherm to the crystallization of magnesium carbonate [7, 8, 18, 24]. In this study, the differential thermal analysis (DTA) curves (Fig. 9) indicate three distinct endothermic events occurring in the temperature range of 200–350, 350–550 and 550–650 °C, which corresponds to the thermal decomposition stages, and only one small exothermic event was observed at the heating rate of 20 °C min⁻¹, it can be concluded that the overall thermal decomposition of hydromagnesite is endothermic, and the presence of an exothermic event depends on the heating

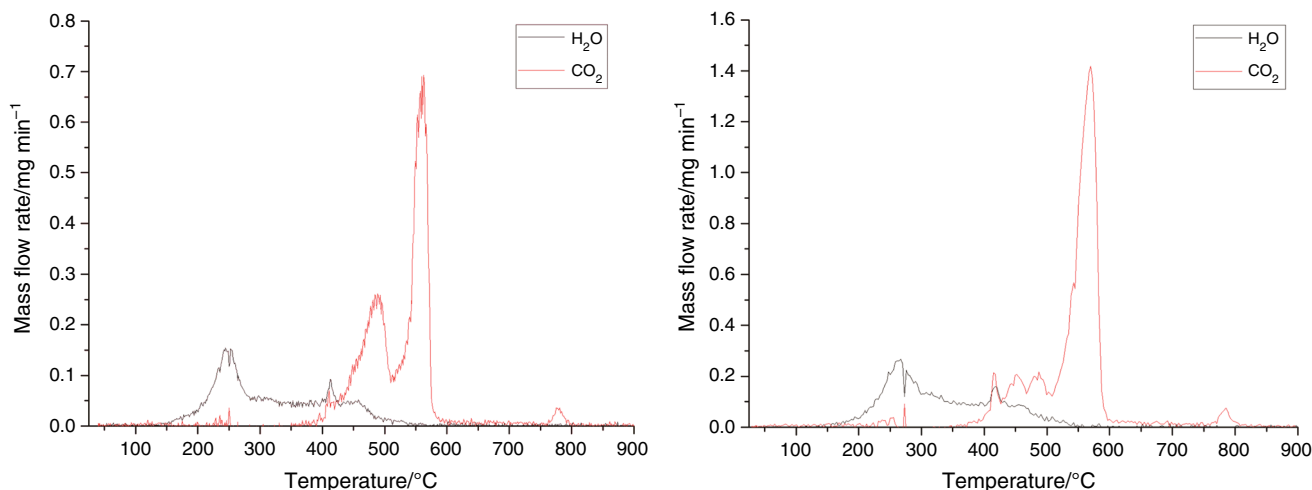


Fig. 8 Analysis of the outlet gases (CO_2 and H_2O) from the decomposition of hydromagnesite in mixed flowing gases atmosphere (helium and carbon dioxide) with a heating rate of $10\text{ }^\circ\text{C min}^{-1}$ (the figure on the left) and $20\text{ }^\circ\text{C min}^{-1}$ (the figure on the right), respectively

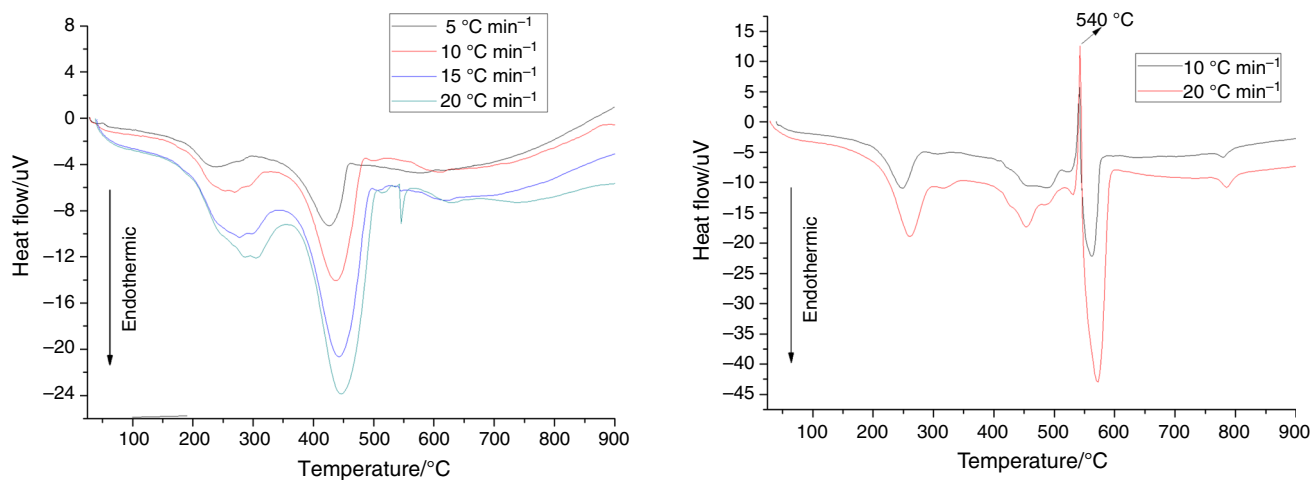


Fig. 9 DTA curves of hydromagnesite in pure flowing helium atmosphere with different heating rates from 25 to $900\text{ }^\circ\text{C}$

rate when measured in a He atmosphere. In addition, this distinct exothermic event was also observed at approximately $540\text{ }^\circ\text{C}$ under a CO_2 atmosphere at a heating rate of $10\text{ }^\circ\text{C min}^{-1}$, which becomes much greater when the heating rate is increased to $20\text{ }^\circ\text{C min}^{-1}$. Combined with the DTA results under He atmosphere, these data clearly show that the presence of this exothermic at around $540\text{ }^\circ\text{C}$ also depends on atmosphere condition. The exothermic event was followed by an endothermic decomposition stage where the released gas was CO_2 at around $560\text{ }^\circ\text{C}$ with a heating rate of $10\text{ }^\circ\text{C min}^{-1}$ and $565\text{ }^\circ\text{C}$ with a heating rate of $20\text{ }^\circ\text{C min}^{-1}$ under CO_2 atmosphere. Figures 5 and 8 obviously show that this endothermic decomposition stage is decarbonation. Thus, this exothermic event occurs due to the crystallization of magnesium carbonate, possibly magnesite, after dehydroxylation

Fig. 10 DTA curves of hydromagnesite in mixed flowing gases atmosphere (helium and carbon dioxide) with different heating rates from 25 to $900\text{ }^\circ\text{C}$

[7, 8, 18, 23]. Therefore, the exothermic crystallization of magnesite occurs at around $540\text{ }^\circ\text{C}$ under conditions of high partial pressure of CO_2 or high heating rates (Fig. 10).

Conclusions

Thermal decomposition characteristics of hydromagnesite from Dujiali Lake, China, were examined using TGA–MS combined with the in situ XRD, SEM and FT-IR. The thermal decomposition characteristics of hydromagnesite show remarkable variations depending on the heating rate and atmospheric conditions. In a He atmosphere, only two decomposition stages were observed, the loss of the crystalline water was followed by the combined dehydroxylation and decarbonation during those decomposition stages,

and the dehydroxylation step overlaps both with the dehydration and decarbonation. However, under a CO₂ atmosphere the decomposition of hydromagnesite occurs in three stages, as the dehydroxylation and decarbonation occur separately due to the inert CO₂ gas preventing the initial decomposition of magnesium carbonate. The overall decomposition of hydromagnesite is endothermic; however, a distinct exothermic event was observed at around 540 °C under conditions of a high partial pressure of CO₂ or high heating rates, which indicates that magnesite is crystallized. Finally, the release of H₂O and CO₂ at different stages likely results from the complex hydrogen bonds and different carbonate groups present in the hydromagnesite structure.

Acknowledgements The authors would like to thank Dr. Hongde Xia and Dr. Kai Wei of the Institute of Engineering, Thermophysics, Chinese Academy of Sciences for experimental support on thermogravimetric analysis/mass spectrometry measurements, and Dr. Zhenfei Lv of the China University of Geoscience for his help with the Fourier transform infrared spectroscopy. This research was supported by The National Key Research and Development Program of China (Grant Number: 2017YFC0602704), National Natural Science Foundation of China (Grant Numbers: 41473061, 41603048 and U1407207) and China Geological Survey (Grant Number: DD20160025).

References

- Power IM, Wilson SA, Harrison AL, Dipple GM, Mccutcheon J, Southam G, et al. A depositional model for hydromagnesite–magnesite playas near Atlin, British Columbia, Canada. *Sedimentology*. 2014;61:1701–33.
- Power IM, Wilson SA, Thom JM, Dipple GM, Gabites JE, Southam G. The hydromagnesite playas of Atlin, British Columbia, Canada: a biogeochemical model for CO₂ sequestration. *Chem Geol*. 2009;260:302–16.
- Lin Y, Zheng M, Ye C. Hydromagnesite precipitation in the Alkaline Lake Dujiali, central Qinghai-Tibetan Plateau: constraints on hydromagnesite precipitation from hydrochemistry and stable isotopes. *Appl Geochem*. 2017;78:139–48.
- Botha A, Strydom CA. Preparation of a magnesium hydroxy carbonate from magnesium hydroxide. *Hydrometallurgy*. 2001;62:175–83.
- Beck CW. Differential thermal analysis curves of carbonate materials. *Am Miner*. 1950;35:985–1013.
- Sawada Y, Uematsu K, Mizutani N, Kato M. Thermal decomposition of hydromagnesite 4MgCO₃—Mg(OH)₂—4H₂O under different partial pressures of carbon dioxide. *Thermochim Acta*. 1978;27:45–59.
- Sawada Y, Yamaguchi J, Sakurai O, Uematsu K, Mizutani N, Kato M. Thermal decomposition of basic magnesium carbonates under high-pressure gas atmospheres. *Thermochim Acta*. 1979;32:277–91.
- Sawada Y, Yamaguchi J, Sakurai O, Uematsu K, Mizutani N, Kato M. Isothermal differential scanning calorimetry on an exothermic phenomenon during thermal decomposition of hydromagnesite 4MgCO₃—Mg(OH)₂—4H₂O. *Thermochim Acta*. 1979;34:233–7.
- Teir S, Eloneva S, Fogelholm CJ, Zevenhoven R. Fixation of carbon dioxide by producing hydromagnesite from serpentinite. *Appl Energy*. 2009;86:214–8.
- Botha A, Strydom CA. DTA and FT-IR analysis of the rehydration of basic magnesium carbonate. *J Thermal Anal Calorim*. 2003;71:987–95.
- Padeste C, Oswald HR, Reller A. The thermal behaviour of pure and nickel-doped hydromagnesite in different atmospheres. *Mater Res Bull*. 1991;26:1263–8.
- Choudhary VR, Pataskar SG, Gunjikar VG, Zope GB. Influence of preparation conditions of basic magnesium carbonate on its thermal analysis. *Thermochim Acta*. 1994;232:95–110.
- Hull TR, Witkowski A, Hollingbery L. Fire retardant action of mineral fillers. *Polym Degrad Stab*. 2011;96:1462–9.
- Vágvölgyi V, Frost RL, Hales M, Locke A, Kristóf J, Horváth E. Controlled rate thermal analysis of hydromagnesite. *J Thermal Anal Calorim*. 2008;92:893–7.
- Haurie L, Fernandez AI, Velasco JI, Chimenos JM, Lopez-Cuesta JM, Espiell F. Effects of milling on the thermal stability of synthetic hydromagnesite. *Mater Res Bull*. 2007;42:1010–8.
- Khan N, Dollimore D, Alexander K, Wilburn FW. The origin of the exothermic peak in the thermal decomposition of basic magnesium carbonate. *Thermochim Acta*. 2001;367–368:321–33.
- Rao TR, Cholan VS. Kinetics of thermal decomposition of hydromagnesite. *Chem Eng Technol*. 2004;18(5):359–363.
- Sawada Y, Uematsu K, Mizutani N, Kato M. Thermal decomposition of hydromagnesite 4MgCO₃·Mg(OH)₂·4H₂O. *J Inorg Nucl Chem*. 1978;40:979–82.
- Hollingbery LA, Hull TR. The fire retardant effects of huntite in natural mixtures with hydromagnesite. *Polym Degrad Stab*. 2012;97:504–12.
- Hollingbery LA, Hull TR. The fire retardant behaviour of huntite and hydromagnesite—a review. *Polym Degrad Stab*. 2010;95(12):2213–2225.
- Realinho V, Haurie L, Antunes M, Velasco JI. Thermal stability and fire behaviour of flame retardant high density rigid foams based on hydromagnesite-filled polypropylene composites. *Compos B Eng*. 2014;58:553–8.
- Laoutid F, Gaudon P, Taulemesse JM, Lopez Cuesta JM, Velasco JI, Piechaczyk A. Study of hydromagnesite and magnesium hydroxide based fire retardant systems for ethylene–vinyl acetate containing organo-modified montmorillonite. *Polym Degrad Stab*. 2006;91:3074–82.
- Hollingbery LA, Hull TR. The thermal decomposition of huntite and hydromagnesite—a review. *Thermochim Acta*. 2010;509:1–11.
- Sawada Y, Yamaguchi J, Sakurai O, Uematsu K, Mizutani N, Kato M. Thermogravimetric study on the decomposition of hydromagnesite 4 MgCO₃·Mg(OH)₂·4H₂O. *Thermochim Acta*. 1979;33:127–40.
- Frost RL, Weier ML, Erickson KL. Thermal decomposition of struvite. *J Therm Anal Calorim* [Internet]. 2004;76:1025–33. <http://download.springer.com/static/pdf/672/art%253A10.1023%252FB%253AJTAN.0000032287.08535.b3.pdf?originUrl=http%3A%2F%2Flink.springer.com%2Farticle%2F10.1023%2FB%3AJTAN.0000032287.08535.b3&token2=exp=1497438534~acl=%2Fstatic%2Fpdf%2F672%2Fart%25253A10.1>.
- Cheng H, Yang J, Liu Q, He J, Frost RL. Thermogravimetric analysis–massspectrometry(TG–MS) of selected Chinese kaolin-ites. *Thermochim Acta* [Internet]. 2010;507–508:106–14. <http://www.scopus.com/inward/record.url?eid=2-s2.0-77955470571&partnerID=tZotx3y1>.
- Paulose S, Thomas D, Jayalatha T, Rajeev R, George BK. TG–MS study on the kinetics and mechanism of thermal decomposition of copper ethylamine chromate, a new precursor for copper chromite catalyst. *J Therm Anal Calorim*. 2016;124:1099–108.

28. Jayaraman K, Kok MV, Gokalp I. Combustion properties and kinetics of different biomass samples using TG–MS technique. *J Therm Anal Calorim.* 2017;127:1361–70.
29. Åkerblom IE, Ojwang DO, Grins J, Svensson G. A thermogravimetric study of thermal dehydration of copper hexacyanoferrate by means of model-free kinetic analysis. *J Therm Anal Calorim.* 2017;129:721–31.
30. Ingram AL, Nickels TM, Maraoulaite DK, White RL. Thermogravimetry–mass spectrometry investigations of montmorillonite interlayer water perturbations caused by aromatic acid adsorbates. *J Therm Anal Calorim.* 2016;126:1157–66.
31. Xia H, Wei K. Equivalent characteristic spectrum analysis in TG–MS system. *Thermochim Acta* [Internet]. 2015;602:15–21. <https://doi.org/10.1016/j.tca.2014.12.019>.
32. Akao M, Marumo F, Iwai S. The crystal structure of hydromagnesite. *Acta Crystallogr Sect B Struct Crystallogr Cryst Chem* [Internet]. 1974;30:2670–2. <http://scripts.iucr.org/cgi-bin/paper?S0567740874007771>.
33. Akao M, Iwai S. The hydrogen bonding of hydromagnesite. *Acta Crystallogr Sect B* [Internet]. 1977;33:1273–5. <http://scripts.iucr.org/cgi-bin/paper?S0567740877005834>.
34. Janet CM, Viswanathan B, Viswanath RP, Varadarajan TK. Characterization and photoluminescence properties of MgO microtubes synthesized from hydromagnesite flowers. *J Phys Chem C.* 2007;111:10267–72.
35. Wang J, Li D, Gao R, Liu Q, Jing X, Wang Y, et al. Construction of superhydrophobic hydromagnesite films on the Mg alloy. *Mater Chem Phys* [Internet]. 2011;129:154–60. <https://doi.org/10.1016/j.matchemphys.2011.03.065>.
36. Zhang Z, Zheng Y, Ni Y, Liu Z, Chen J, Liang X. Temperature- and pH-dependent morphology and FT-IR analysis of magnesium carbonate hydrates. *J Phys Chem B.* 2006;110:12969–73.
37. Gil Kim S, Hyun Choi K, Hwan Eun J, Joon Kim H, Seung Hwang C. Effects of additives on properties of MgO thin films by electrostatic spray deposition. *Thin Solid Films.* 2000;377–378:694–8.